**Proceedings of the 28th IEEE**
**EMBS Annual International Conference**
**New York City, USA, Aug 30-Sept 3, 2006**



# Nosologic Maps of Brain Tumor Images Obtained from Combination of Different MRI Modalities

Miguel Martín-Landrove, *Member, IEEE*

***Abstract*— Tissue classification is a necessary step to obtain the spatial distribution of a pathology or nosologic map and typically it is performed by the combination of different medical image modalities, including histopathological studies. In previous work, combination of different magnetic resonance (MR) modalities such as *in vivo* spectroscopy, relaxometry and diffusometry have been proposed to obtain nosologic maps with appropriate spatial resolution for treatment considerations. Due to the low spatial resolution of localized *in vivo* spectroscopy and low longitudinal resolution in relaxation and diffusion-weighted images a partial volume problem is always present. Present work attempts to overcome this problem by careful analysis of transversal relaxation rate and apparent diffusion coefficient distributions obtained by an Inverse Laplace Transform Algorithm (ILTA).**

## I. Introduction

MAGNETIC Resonance Spectroscopy (MRS) is a non-invasive tool that allows distinguishing brain malignant tumors from non-anaplastic tumors [1], and is able to detect significant differences between in vivo spectra of tumor, necrosis and normal brain tissue [2], [3]. Nosologic maps [4] can be obtained by the Chemical Shift Imaging (CSI) technique but they lack the spatial resolution necessary for therapy planning and follow up. Relaxation studies have been used long ago for the assessment of tumors, being $T_2$-weighted images the basis for clinical diagnosis. Diffusion-weighted MRI has been used to distinguishing different tissue components in brain tumors [5]. Due to the heterogeneity of tumoral lesions and voxel size, a partial volume problem [6], is always present and suitable numerical techniques are needed to separate the different tissue components [7]. In previous work [8], [9], [10], nosologic maps are obtained by the combination of MRS and relaxometry. In the present work, it is established a comparison between different tissue classification schemes and MRI modalities to obtain reliable nosologic maps.

## II. Materials and Methods

### A. Image Measurements

Different MRI modalities were used in this work. To obtain localized *in vivo* spectroscopy information, CSI was performed axially with TE = 30 ms and VOI of 96 $cm^3$ (80x80x15 mm) centered at the tumor lesion. Structural studies included the acquisition of multiecho $T_2$-weighted images using the Carr-Purcell-Meiboom-Gill (CPMG) sequence with 16 echoes, a base echo time TE = 22 ms and 8 axial image slices 5mm thick. Diffusion-weighted images were obtained for 16 b-parameter values ranging from 0 to 1350 $s/mm^2$ and 3 orthogonal magnetic gradient directions (Phase, Read and Slice). Image parameters for the structural studies were taken the same that the CSI study in such a way that 2 slices were included inside the CSI grid. The pixel intensity for the structural images is generally given by

$$I(\alpha) = I_0 \exp(-\alpha\rho) \tag{1}$$

where $\alpha = nTE$, $\rho = 1/T_2$ for $T_2$-weighted images; $n$ being the echo index and $T_2$ the transversal relaxation time, and $\alpha = b_i$, $\rho = D_{ii}$ for diffusion-weighted images; $i = p, r, s$ stands for the direction of the gradient and $D_{ii}$ represents the corresponding diagonal component of the diffusion tensor, the sequence parameter $b_i$ is

$$b_i = \gamma^2 G_i^2 \delta^2 (\Delta - \delta/3) \tag{2}$$

where γ is the gyromagnetic ratio, $G_i$ is the magnitude of gradient pulses, δ is the gradient pulse width and Δ is the time interval between pulses.

### B. The Partial Volume Problem

The fact that the size of a localized *in vivo* spectroscopy voxel is big enough to contain more than one tissue type introduces a partial volume problem. The same happens when other MRI modalities are considered since even when the axial spatial resolution, i.e., over the 2D image, is very high, the longitudinal spatial resolution, i.e., slice width, is very low. As a consequence, it can be assumed that there is a distribution of parameters within the image voxel. In that case the image intensity in a voxel can be written as

$$I(\alpha) = \int_0^\infty d\rho\, e^{-\alpha\rho} P(\rho) \tag{3}$$

In order to solve (3) for $P(\rho)$, an Inverse Laplace Transform Algorithm (ILTA) was developed [8] assuming a simple proposition for the distribution $P(\rho)$

Manuscript received April 3, 2006.

M. Martín-Landrove is with the Centro de Física Molecular y Médica, Escuela de Física, Facultad de Ciencias, Universidad Central de Venezuela (phone: +58-212-6051194; fax: +58-212-6051516; e-mail: mmartin@fisica.ciens.ucv.ve).

$$P(\rho)=\sum_{k=1}^{N} P_k(\rho) \tag{4}$$

where $N$ is the total number of components, and $P_k(\rho)$, the kth elemental component given by

$$P_k(\rho)=P_k\Theta(\rho-\rho_k)\Theta(\rho_k+\Delta\rho_k-\rho) \tag{5}$$

with Θ, the step function. This representation can be used for the description of either discrete or continuous distributions. The problem to be solved can be stated as an optimization procedure where a set of distribution components, which provides the best fit for the $I(\alpha)$ function, has to be found. For that purpose simulated annealing and Metropolis algorithms [11,12], are used. The configuration to be tested in each Metropolis algorithm cycle is given by a finite number of elementary components that are sampled in the decay rate position $\rho_k$ and width $\Delta\rho_k$

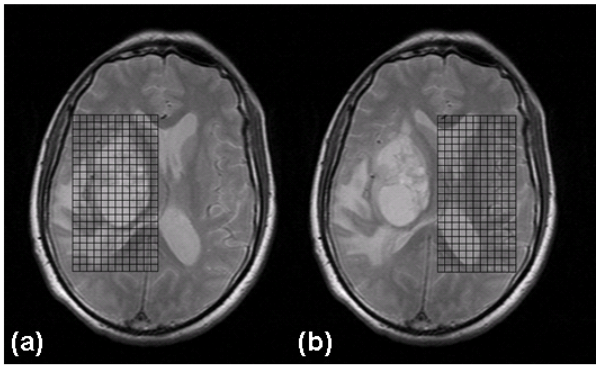


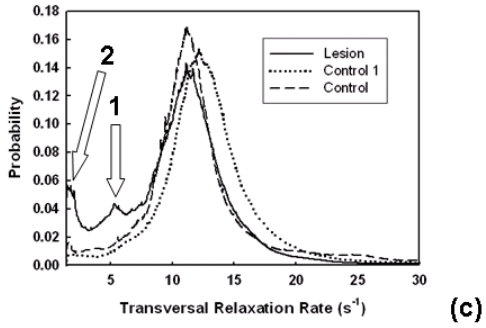


Fig. 1. Sampling of relaxation data on $T_2$-weighted images: (a) VOI over the lesion, (b) VOI over an unaffected region on the same slice, (c) Transversal relaxation rate distributions: continuous line corresponds to the lesion, dotted line is a control case (healthy volunteer) and dashed line corresponds to the unaffected tissue. Arrows indicate differences, 1 is related to tumoral tissue and 2 to cerebrospinal fluid or necrosis, determined by i*n vivo* spectroscopy.

for the kth element. At the same time, the total number of components $N$ for the configuration is also changed. Optimization ends minimizing the quantity

$$\Delta=\frac{1}{n_P}\sum_{i=1}^{n_P}\frac{\left|I_{\exp}(\alpha_i)-I_{op}(\alpha_i)\right|}{\left|I_{\exp}(\alpha_i)\right|} \tag{6}$$

As it is conmmon in this type of optimization procedures, search in the parameters space depends on the appropriate selection of initial conditions. Up to 300 random selection of initial conditions were used to obtain $P(\rho)$. The distribution functions can be obtained from a single voxel (size depending on the image modality used) or a volume of interest (VOI) including various voxels. In Figure 1, it is shown an example of the application of this procedure to $T_2$-weighted images.

### C. Tissue Classification and Nosologic Maps

Tissue classification was established by the evaluation of metabolite relative concentrations coming from localized *in vivo* spectroscopy data. Two metabolites are considered significant, Choline (Cho), related to cellular proliferation and N-Acetyl-Aspartate (NAA) related to neuron population. For a Cho/NAA ratio [13]: greater than 1.3, the tissue was considered malignant, within the range 0.9 to 1.29, atypical and below 0.9 it was considered unaffected. If all metabolites exhibit low concentrations the tissue can be classified as necrotic. In the case that no spectroscopic information is available, other factors are used for tissue classification depending on the MRI modality used, for example, in diffusion-weighted images; the diffusion tensor anisotropy can be used as a good estimator to separate unaffected tissue from others in the lesion. Also, a comparison between different image regions, as shown in Figure 1 can be helpful for tissue classification.

In order to obtain the nosologic map, the classified tissue

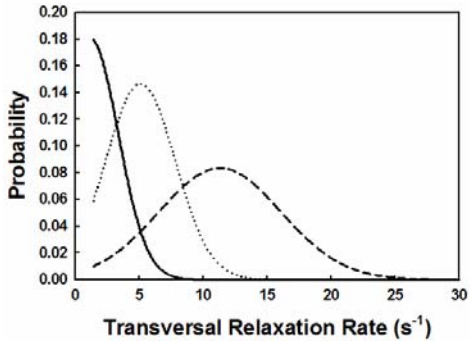


Fig. 2. Probability distributions obtained from comparison in Figure 1c and validated by localized *in vivo* spectroscopy: continuous line represents necrosis or cerebrospinal fluid, dotted line represents tumoral tissue and dashed line represents normal or unaffected tissue. All probability distribution functions are normalized

types have to be identified on the image. This is generally done by decomposing $P(\rho)$ in a set of probability distributions each one associated to a tissue type, as shown in Figure 2. Probability distributions so obtained can be used in different ways to obtain nosologic maps.

#### 1) Method 1. Nosologic maps obtained by linear regression.

One approach, used in [9], [10], assumes that image

intensity for each voxel is a linear superposition of decaying exponential functions, each one characterized by a decay parameter ρ, taken as the mean value ‹ρ› of the probability distribution for each classified tissue type

$$I(\alpha) = bl + \sum_i A_i X_i(\alpha) \tag{7}$$

with

$$X_i(\alpha) = \exp\left(-\langle \rho \rangle_i \alpha\right) \tag{8}$$

*bl* is a parameter introduced to take into account corrections in the baseline of the image intensity decay and the coefficients $A_i$, which are positive, determine the proportion of each decay in the image. Equation (8) is fitted by a linear regression procedure and the coefficients $A_i$ were accepted only if a minimum correlation coefficient squared, $r^2$, was attained. Since exponential functions are correlated, minimum $r^2$ values are taken starting at 0.990. The dependence of the nosologic map on $r^2$ is shown in Figure 3. Gray levels are assigned based on the coefficients $A_i$, and sometimes a RGB color code can be defined [10].

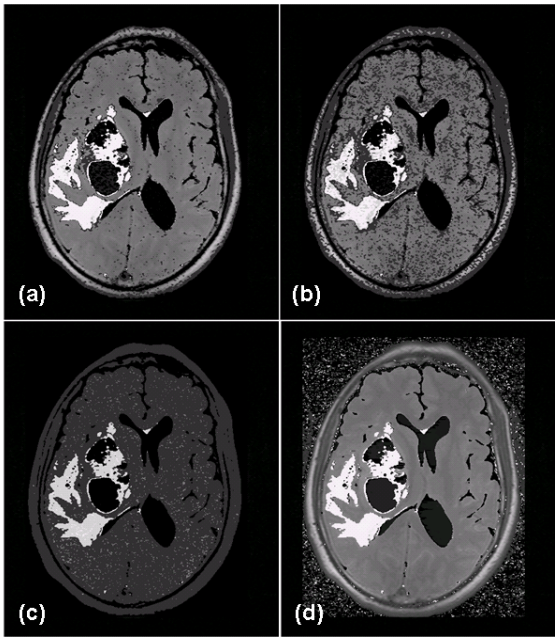


Fig. 3. Nosologic maps obtained by linear regression analysis. Dark gray levels correspond to liquid or necrosis, gray to unaffected tissue and light gray to tumor presence. In all maps gray levels are assigned for that tissue with maximum coefficient in the linear regresion analysis: (a), (b) and (c) additionaly consider maximum $r^2$ greater than 0.990, 0.995 and 0.999 respectively; (d) is independent on $r^2$.

*2) Method 2. Nosologic maps obtained by nonlinear regression.*

The probability distributions obtained by the application of ILTA are characterized not only by their mean values ‹ρ›, but also by their dispersions, σ, (see Figure 2), which are dependent on signal to noise ratios and tissue heterogeneity, i.e., unaffected tissue is dispersed in the parameter ρ due to differences in the parameter for gray and white matter tissues. Assuming that tissue type probability distributions reflect the actual distribution of the parameter ρ, then its value in a voxel could be used to determine the probabilities for each tissue type. If it is assumed that, in a voxel

$$I(\alpha) = bl + C\exp\left(-\alpha\tilde{\rho}\right) \tag{9}$$

where bl has been defined previously and $\tilde{\rho}$ represents an "average" of the parameter in the voxel. To obtain $\tilde{\rho}$, a non linear regression analysis, made by the Levenberg-Marquardt method [14], [15] is applied on each voxel. Tissue probabilities are calculated by

$$p_i(\tilde{\rho}) = \exp\left(-\left(\tilde{\rho} - \langle \rho \rangle_i\right)^2 / 2\sigma_i^2\right) / \sigma_i\sqrt{2\pi} \tag{10}$$

Nosologic maps are obtained normalizing tissue probabilities $p_i$ within the voxel. Figure 4 shows the results for this procedure. It is also possible to obtain nosologic maps for each tissue type, as shown in Figure 5

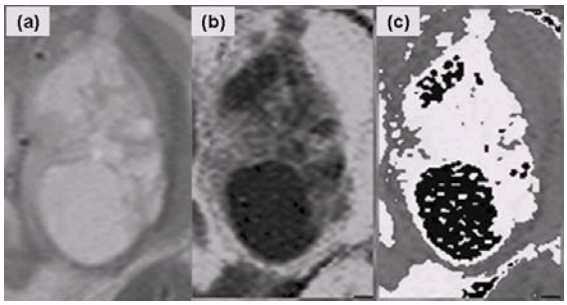


Fig. 4. Nosologic maps obtained by nonlinear regression analysis. (a) Original $T_2$-weighted image, (b) nosologic map using a gray level palette proportional to the normalized tissue probability, dark gray corresponds to liquid or necrosis and light gray to unaffected tissue, (c) nosologic map representing only the tissue type with maximum normalized tissue probability; gray levels are defined as in Figure 3.

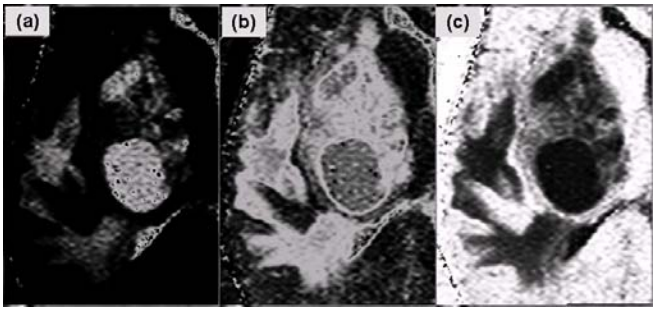


Fig. 5. Nosologic maps for each tissue type. (a) Liquid or necrosis, (b) tumor and (c) unaffected tissue. Gray scale is proportional to normalized tissue probability.

## III. Results and Discussion

Both methods described in this work provide nosologic maps that attempt to solve the partial volume problem which is characteristic of the MRI modalities employed. In general,

the analysis of the structural images by.ILTA on which both methods are based provides the tissue classification and tissue probability quantification that allows for the construction of nosologic maps, even in the case when localized *in vivo* spectroscopy is not possible, due to organ movement or poor magnetic field homogeneity.

Method 1, which uses linear regression analysis, was disscused in detail in [10]. Due to the fact that exponential functions are correlated some voxels, particularly those in the interface between cerebrospinal fluid and unaffected tissue are take as tumor positive in the nosologic map, i.e., the mean transversal relaxation rate for tumoral tissue lies between those of liquid and unaffected tissue, and this situation imposes additional criteria to obtain the nosologic map [10]. Nevertheless, its application is faster and can be used as a method for total image inspection prior to more detailed analysis, particularly in tumor boundary.

Method 2 takes into account the tissue type probability densities defined in (10) but as can be seen in Figure 2, there are considerable overlap among them which is responsible for the appearance of tumor positive voxels, particularly in tissue interfaces. Other aspect to be considered is how $\widetilde{\rho}$ is evaluated, which imposes a particular model function (9) for the image intensity in the voxel. A more refined method should apply ILTA to the voxel data and project the distribution function on the tissue type probability density set to determine tissue proportions within the voxel. Unfortunately, the precision of ILTA to determine the actual distribution of the parameter depends on a high number of initial conditions and as consequence its use is limited to few voxels, unless a parallel code could be implemented.

## IV. Conclusions

Nosologic maps can be obtained using a single medical imaging modality (MRI) combining different studies. Simple registration algorithms are used for image fusion since the patient is not repositioned in a different medical image equipment. No markers, either fiducial or anatomical, are needed, only corrections related to different spatial resolutions and very small movement artifacts. Analysis of structural image data by an inversion algorithm (Inverse Laplace Transform) allows for tissue classification and contributes to solve the partial volume problem providing nosologic maps of higher spatial resolution compared to localized spectroscopic data. The method provides a quantitative tool to evaluate gross tumor volume or GTV for treatment planning and treatment follow up. Nosologic maps can be used as input DICOM images in 3D planning systems. Other MRI studies can be incorporated, such as perfusion and MR angiography. MRI processed images can be registered to different medical imaging modalities, such as SPECT or PET/CT to fully assess for tumor presence and parametrization. Extension to other organs, such as prostrate and breast, is possible. In cases where in vivo spectroscopy is not possible, relaxation, diffusion, perfusion or angiography studies could be used to construct the nosologic map.

## Acknowledgment

The author would like to thank the collaboration of technical and medical staff of the Instituto de Resonancia Magnética, La Florida/San Román in Caracas, Venezuela and the financial support of the Universidad Central de Venezuela.

## References

[1] M. Castillo and L. Kwock, "Proton MR spectroscopy of common brain tumors", *Neuroimag. Clin. North Am.*, vol. 4, pp. 733-752, 1998.

[2] F.A- Howe, S.J. Barton, S.A. Cudlip, M. Stubbs, D.E. Saunders, M. Murphy, P. Wilking, K.S. Opstad et al., "Metabolic profiles of human brain tumors using quantitative in vivo 1H magnetic resonance spectroscopy", *Magnetic Resonance in Medicine*, vol. 49, pp. 223-232, 2003.

[3] S.J. Nelson, "Multivoxel magnetic resonance spectroscopy of brain tumors", *Mol. Cancer Ther.*, vol. 2, pp. 497-507, 2003.

[4] F. Szabo de Edelenyi, C. Rubin, F. Esteve, S. Grand, M. Decorps, V. Lefournier, J.-F. Le Bas and C. Remy, "A new approach for analyzing proton magnetic resonance spectroscopic images of brain tumors:nosologic images", *Nat. Med.*, vol. 6, pp. 1287-1289, 2000.

[5] S.E. Maier, P. Bogner, G. Bajzik, H. Mamata, Y. Mamata, I. Repa, F.A. Jolesz and R.V. Mulkern, "Normal brain and brain tumor: multicomponent apparent diffusion coefficient line scan imaging", *Radiology*, vol. 219, pp. 842-849, 2001.

[6] M. Pokric, N. Thacker, M.L.J. Scott and A. Jackson, "The importance of partial voluming in multi-dimensional medical image segmentation", in *MICCAI 2001*, Niessen, W. & Viergever, M., eds., LNCS 2208, Springer-Verlag, 2001.

[7] K. Van Leemput, F. Maes, D. Vandermeulen and P. Suetens, "A unifying framework for partial volume segmentation of brain MR images", *IEEE Transactions on Medical Imaging*, vol. 22, pp. 105-119, 2003.

[8] R. Martín and M. Martín-Landrove, "A novel algorithm for tumor characterization by analysis of transversal relaxation rate distributions in MRI", in *Spatially Resolved Magnetic Resonance*, Blümler, P., Blümich, B., Botto, R., Fukushima, E., eds., chap. 11, pp. 133-138, Wiley-VCH, 1998.

[9] M. Martín-Landrove, I. Bautista, F. Mayobre, R. Villalta, and A. Contreras, "Tumor assessment by in vivo proton spectroscopy and relaxometry", *Magma*, vol. 15, pp. 225-226, 2002.

[10] M. Martín-Landrove, F. Mayobre, I. Bautista and R. Villalta, "Brain tumor evaluation and segmentation by in vivo proton spectroscopy and relaxometry", *MAGMA*, vol. 18, pp. 316-331, 2005.

[11] G. Bhanot, "The Metropolis algorithm", *Rep. Prog. Phys.*, vol. 51, pp. 429-457, 1988.

[12] S. Kirkpatrick, C.D. Gellatt and M.P. Vecchi, "Optimization by simulated annealing", *Science*, vol. 220, pp. 671-680, 1983.

[13] S.Nelson, D. Vigneron and W. Dillon, "Serial evaluation of patients with brain tumors using volume MRI and 3D $^{1}$H MRSI", *NMR Biomed.*, vol. 12, pp. 123-138, 1999.

[14] K. Levenberg, "A method for the solution of certain problems in least squares", *Quart. Appl. Math.*, vol. 2, pp. 164-168, 1944.

[15] D. Marquardt, "An algorithm for least squares estimation of nonlinear parameters", *SIAM J. Appl. Math.*, vol. 11, pp. 431-441, 1963.